Integrated Systems and Technologies

Cancer Research

In Vivo Diagnosis of Melanoma and Nonmelanoma Skin Cancer Using Oblique Incidence Diffuse Reflectance Spectrometry

Alejandro Garcia-Uribe[1,2], Jun Zou[2], Madeleine Duvic[3], Jeong Hee Cho-Vega[4], Victor G. Prieto[4], and Lihong V. Wang[1]

Abstract

Early detection and treatment of skin cancer can significantly improve patient outcome. However, present standards for diagnosis require biopsy and histopathologic examinations that are relatively invasive, expensive, and difficult for patients with many early-stage lesions. Here, we show an oblique incidence diffuse reflectance spectroscopic (OIDRS) system that can be used for rapid skin cancer detection *in vivo*. This system was tested under clinical conditions by obtaining spectra from pigmented and nonpigmented skin lesions, including melanomas, differently staged dysplastic nevi, and common nevi that were validated by standard pathohistologic criteria. For diagnosis of pigmented melanoma, the data obtained achieved 90% sensitivity and specificity for a blinded test set. In a second analysis, we showed that this spectroscopy system can also differentiate nonpigmented basal cell or squamous cell carcinomas from noncancerous skin abnormalities, such as actinic keratoses and seborrheic keratoses, achieving 92% sensitivity and specificity. Taken together, our findings establish how OIDRS can be used to more rapidly and easily diagnose skin cancer in an accurate and automated manner in the clinic. *Cancer Res; 72(11); 2738–45. ©2012 AACR.*

Introduction

Skin cancer is the most common form of cancer, with about a million new cases in the United States each year (1). Often, skin cancer is difficult to diagnose noninvasively, as malignant skin lesions can closely resemble their benign counterparts. Different lesion types can have similar characteristics, furthering the problem in discriminating among them. Among all the skin lesions, melanoma is the most malignant type and is the leading cause of death from the skin diseases. The American Cancer Society estimates that there will be approximately 62,000 new cases of melanoma in the United States this year, with about 8,000 deaths (1). Melanoma can be mistaken for common nevi, dysplastic nevi, and seborrheic keratoses. Common nevi are benign moles formed by a cluster of melanocytes in the basal layer of the epidermis or in the top layers of the dermis. Dysplastic nevi are moles with atypical size, shape, or organization. Depending on the degrees of atypia, dysplastic nevi can be mild, moderate, or severe. Dysplastic nevi are more likely than common nevi to develop into melanomas (2). Finally, seborrheic keratoses are benign wart-like tumors that are very common in people older than 40 years.

In addition to melanoma, skin cancers also include squamous cell carcinomas (SCC) and basal cell carcinomas (BCC). Squamous cell carcinomas arise from dividing keratinocytes of the epidermis and are often recognized by hyperkeratotic crusts or scales or by ulceration in the later stages. Actinic keratosis, a precancerous skin tumor caused by sun exposure, can in some cases turn into SCC, which in invasive cases may metastasize to local nodes and beyond (3). BCCs are derived from keratinocytes (4). BCCs are locally invasive, slow-growing tumors characterized by islands or nests of basal keratinocytes invading the dermis. There are several clinical and histologic subtypes of BCCs. Superficial BCCs are papulosquamous lesions characterized by red, scaly raised plaques.

Early detection and treatment of skin cancer can significantly improve patient outcomes. In clinical practice, visual examination determines whether a skin lesion is cancerous based on the ABCDE rule (asymmetry, border, color, diameter, and evolution) and the change in the appearance of a mole or pigmented area over a period of time. However, clinical diagnostic sensitivity and specificity vary greatly, depending on the expertise and visual skills of the clinician. Consequently, histopathologic examination of the excised suspicious element still remains the gold standard. However, biopsy is an invasive procedure and leaves a scar at the biopsy site, which otherwise would be unnecessary in the case of benign lesions. Moreover, the removal of every lesion can be unacceptable for patients with large numbers of skin abnormalities, such as in dysplastic nevi syndrome.

Authors' Affiliations: [1]Department of Biomedical Engineering, Washington University in St. Louis, St. Louis, Missouri; [2]Department of Electrical and Computer Engineering, Texas A&M University, College Station; and Departments of [3]Dermatology and [4]Pathology, The University of Texas MD Anderson Cancer Center, Houston, Texas

Corresponding Authors: Lihong V. Wang, Washington University in St. Louis, One Brookings Drive, Whitaker Hall, Campus Box 1097, St. Louis, MO 63130. Phone: 314-935-7208; Fax: 314-935-7448; E-mail: lhwang@wustl.edu; and Alejandro Garcia-Uribe, E-mail: aguribe@gmail.com

doi: 10.1158/0008-5472.CAN-11-4027

Changes in the cell nuclear matrix have been associated with cell and tissue structures, which are important features in the diagnosis of cancer (5, 6). Morphologic changes in tumor cells include alterations of nuclear structure such as changes in nuclear size and shape (5). These alterations are important characteristics used in cancer diagnosis. Cell nuclei, mitochondria, other cytoplasmic organelles, and cell nuclei are the major light scatterers in the skin tissue. In malignant tissues, larger atypical nuclei and larger cell volume are a main cause for the significant increase in the light scattering (7). For example, the reduced scattering coefficient has been shown to generally increase with the degree of dysplasia or malignancy of skin lesions (8).

Recently, noninvasive spectroscopic methods for tissue diagnosis have been studied for a number of organ systems, including the skin (9–17), gastrointestinal tract (18–22), cervix (23–25), and breast (26–28). The absorption of light can provide information of the biochemical composition of the skin. The light scattering properties of skin can provide information about its microarchitecture (29). Fluorescence spectroscopy can detect disease states (30, 31). Because fluorescence is a manifestation of the biochemical environment of the cell, it should be a specific indicator of cellular alterations caused because of disease (32). Some studies also suggest that Raman spectroscopy can detect changes in protein and lipid structure that can be used to diagnose skin tumors (13). In this study, we report the use of spatially resolved oblique incidence diffused reflectance spectroscopy (OIDRS) as a noninvasive tool to discriminate melanoma and nonmelanoma skin cancer from benign and premalignant skin lesions *in vivo*. Spatiospectral diffuse reflectance data within the wavelength range of 455 to 765 nm was collected from multiple types of pigmented and nonpigmented skin lesions ($n = 678$). The data were used in combination with artificial neural network (ANN) analysis to separate skin cancers such as pigmented malignant melanoma and nonpigmented BCCs and SCCs from their benign counterparts. Neural networks are particularly helpful for classification. ANN classifiers are more powerful than common statistical classifiers because they do not need hypothesis about data distribution, linearity, or correlations (33). ANNs provide better prediction accuracy and higher sensitivity and specificity with optimal use of the available information.

Materials and Methods

Figure 1 is a schematic of the experimental OIDRS system. The system was built onto a portable cart; it was easily moved to the patient examination rooms. To target both small and large skin lesions, we constructed an optical fiber probe using micromachining technology. The probe consisted of 3 source fibers and 2 linear arrays of 12 collection fibers within an area of 2×2 mm^2. To conduct OIDRS measurements on skin lesions, the optical probe was placed gently on the skin area of interest without significant compression. The optical multiplexer delivered light through only one oblique source fiber at a time to the area of interest. Once the light was delivered to the skin, it interacted with the skin tissue, and the spatially resolved diffuse reflectance was collected by one set of collection fibers.

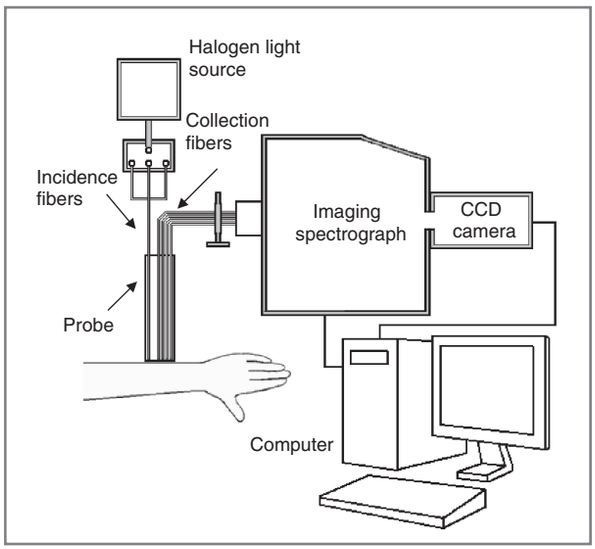

Figure 1. A schematic of the experimental OIDRS system.

The collection fibers were coupled to an imaging spectrograph that generated an optical spectrum from 455 to 765 nm for the collection channel. A charge-coupled device (CCD) camera collected the spectral images, which were stored on a computer for data analysis. The data collection took less than 5 minutes, and it did not interfere with the standard health care provided to the patients.

Data were collected at the University of Texas MD Anderson Cancer Center (Houston, TX). A physician identified the lesion (s) to be measured before the scheduled biopsy. To average out the effect of structural anisotropy of the skin tissue, the measurement of each lesion was repeated 4 times to obtain images from different orientations. To provide self-references, the same measurements were also repeated on the neighboring healthy skin tissues. The anisotropy is defined as the variation of the measurements when conducted in different directions. After the measurements were completed, a biopsy was carried out for each skin lesion and submitted for histopathologic analysis. The histopathologic analysis determined that the measured pigmented lesions consisted of benign common nevi, mildly dysplastic nevi (DN1), moderately dysplastic nevi (DN2), severely dysplastic nevi (DN3), and melanomas. The criteria used to divide dysplastic nevi into these tree categories are described in the work of Shea and colleagues 34. Of the 407 pigmented skin lesions, 271 were used for the training sets of ANN classifiers (Tables 1 and 2) to separate malignant melanoma from varieties of nevi. The remaining 136 data sets were used to test the efficacy of the ANN classifiers. The nonpigmented lesions consisted of BCCs, SCCs, benign actinic keratoses, and seborrheic keratoses. Among the 266 nonpigmented lesions, 177 were used to train the ANN classifier and the remaining 89 were used for testing.

Results

The absorption coefficient (μ_a) and reduced scattering coefficient (μ_s') of the skin lesions from the measured diffuse

Table 1. Pigmented lesions confusion matrix

	Predicted					
Actual	**M**	**DN3**	**DN2**	**DN1**	**CN**	**Total**
Training						
MM	20	0	0	0	0	20
DN3	1	28	0	0	0	29
DN2	4	2	118	2	1	127
DN1	3	1	0	33	1	38
CN	4	2	2	1	48	57
Testing						
MM	9	0	1	0	0	10
DN3	2	12	1	0	0	15
DN2	6	2	53	2	0	63
DN1	1	1	0	16	2	20
CN	4	1	1	0	22	28

Abbreviations: CN, common nevi; DN1, mildly dysplastic nevi; DN2, moderately dysplastic nevi; DN3, severely dysplastic nevi; M, melanomas.

reflectance were estimated on the basis of a combination of both diffusion theory and scalable Monte Carlo simulation (35, 36). Because the optical transport mean free path (L_t') is a function of the wavelength of the incident light, the location of the detectors may fall either within or outside the range of L_t' at different wavelengths within the wide spectrum (455–765 nm). At certain wavelengths, when the location of the detectors falls outside the range of L_t', the absorption and scattering optical properties of the skin lesion can be directly calculated from diffuse reflectance with a straightforward diffusion theory–based analytic model. However, this model would fail at other wavelengths when the detector location falls within L_t'. In this case, scalable Monte Carlo simulation was conducted to deduce the absorption and scattering optical properties of the skin lesions in an inverse problem by calculating and matching the simulated diffuse reflectance results with the actual measurements.

The optical properties of human skin vary significantly between locations and individuals, depending on race, age, sun exposure, and skin type. Figure 2A and B show the μ_a for the statistically significant skin types included in this study. We reduced these variations by measuring and subtracting the optical priorities from the surrounding healthy skin for each lesion. The differential absorption coefficient spectrum is defined as

$$\Delta\mu_a(\lambda) = \mu_a(\lambda)_L - \mu_a(\lambda)_N \quad (A)$$

where $\mu_a(\lambda)_L$ and $\mu_a(\lambda)_N$ are the absorption coefficient spectra measured from the lesion and from the normal surrounding skin, respectively. In a similar way, the differential reduced scattering coefficient is defined as

$$\Delta\mu_s'(\lambda) = \mu_s'(\lambda)_L - \mu_s'(\lambda)_N \quad (B)$$

Figure 2 shows the average absorption coefficient $\mu_a(\lambda)_L$, differential absorption coefficient $\Delta\mu_a(\lambda)$, reduced scattering coefficient $\mu_s'(\lambda)_L$, and differential reduced scattering coefficient $\Delta\mu_s'(\lambda)$ for melanoma, dysplastic nevi, and common nevi, respectively.

The diffuse reflectance of tissue is related largely to absorption and scattering. Mitochondria, cell nuclei, and other cytoplasmic organelles are known changeable parameters in cancerous tissues and are major light scatterers in skin tissue (37, 38). Although no single histologic variable specifically distinguishes these types of pigmented lesions, nuclear atypia seems directly related to the amount of light scattering. Dysplastic nevi are characterized by nuclear enlargement, slight irregularity, and hyperchromasia, with clumping of chromatin and sometimes with prominent nucleoli. Dysplastic nevi present atypical features that are both clinically and histologically important as simulants of melanoma. Like other cancers, most malignant melanomas evolve through a number of stages of tumor progression. Clinically, many melanomas begin as a pigmented patch of skin, which evolves to become a palpable plaque, and enlarges, as if it were along the radii of an imperfect circle (39). Nests and single melanocytes of variable sizes shapes are present in the epidermis in a pagetoid pattern, characteristic of superficial melanoma. Prognosis has long been known to correlate with melanoma thickness as measured microscopically. These factors can increase the contribution of scattering to the diffuse reflection on the surface.

Table 2. Sensitivity and specificity for each classifier included in the hierarchical classification scheme

	Training		Testing		Overall	
	Sensitivity	**Specificity**	**Sensitivity**	**Specificity**	**Sensitivity**	**Specificity**
MM vs. (DN3 DN2, DN1, CN)	100%	95%	90%	90%	97%	93%
DN3 vs. (DN2, DN1, CN)	100%	98%	92%	96%	98%	97%
DN2 vs. (DN1, CN)	98%	98%	96%	98%	97%	98%
DN1 vs. CN	97%	98%	89%	100%	94%	99%

Abbreviations: CN, common nevi; DN1, mildly dysplastic nevi; DN2, moderately dysplastic nevi; DN3, severely dysplastic nevi; M, melanomas.

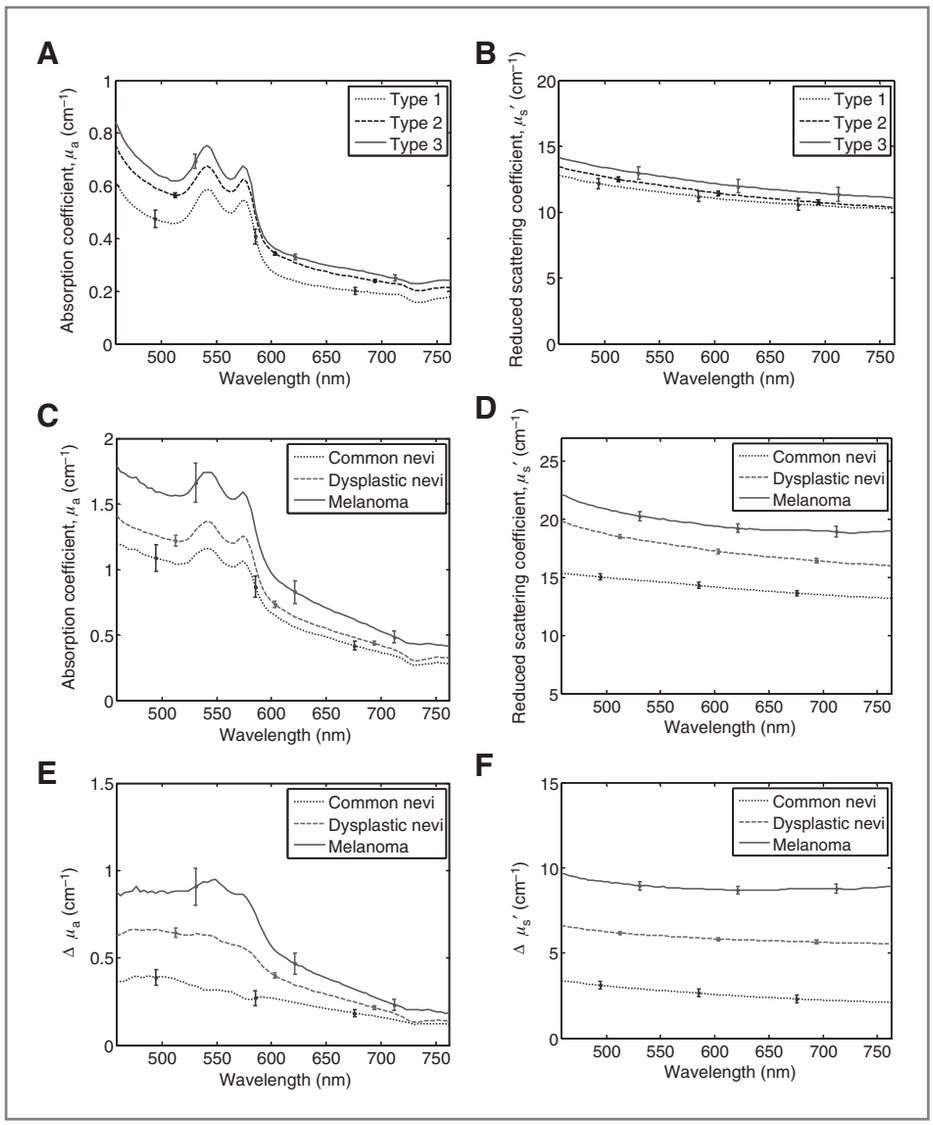

Figure 2. Average absorption coefficient spectra $\mu_a(\lambda)$ (A) and average reduced scattering coefficient (B) for skin types 1, 2, and 3 estimated from 47, 816, and 44 lesions, respectively. C, average absorption coefficient spectra. D, average reduced scattering coefficient spectra. Average differential absorption coefficient spectra (E) and average differential reduced scattering coefficient spectra (F) for common nevi, dysplastic nevi, and melanoma. The error bars represent SEs.

A one-way ANOVA test was carried out to compare $\mu_a(\lambda)_L$ for common nevi, dysplastic nevi, and melanoma. The P value was significant ($P < 0.01$) in the spectral region between 488 and 576 nm. Pairwise comparisons using Tukey test showed a significant difference only between common nevi and melanoma. A similar analysis for $\mu_s'(\lambda)_L$ shows a significant difference of at least one mean for the entire wavelength range (455–765 nm). The ANOVA test of the $\Delta\mu_a(\lambda)$ showed statistical difference in the range between 455 and 599 nm, with the lowest P value at 556 nm ($P = 0.00063$). The pairwise comparisons revealed that $\Delta\mu_a(\lambda)$ from 549 to 556 nm presented a significant difference among the 3 types of lesions. This spectral region corresponds to an absorption peak in deoxyhemoglobin. These results showed the importance of subtracting the optical properties of the surrounding healthy skin for each lesion to reduce the variations due to differences in skin type and condition. The ANOVA and Tukey tests of $\Delta\mu_s'(\lambda)$ show a significant difference among the 3 types of lesions when using the spectral range between 455 and 765 nm. Both SCCs and BCCs presented on average a higher differential reduced scattering coefficient than actinic keratosis and seborrheic keratosis (Fig. 3). An ANOVA and Tukey test of $\mu_a(\lambda)_L$ revealed no significant difference among all 4 types of lesions. However, the ANOVA test of $\Delta\mu_a(\lambda)$ showed a P value that indicates a significant difference ($P < 0.01$) in the spectral region of 455 to 633 nm with the lowest $P = 0.0008$ at 577 nm. The absorption coefficient spectra for seborrheic keratoses have the largest variation (Fig. 3). The subtraction of the reference absorption coefficients from the lesions' absorption coefficients reduces the overlap among the types of lesions and resulted in a statistically significant difference between actinic keratoses, SCCs, and BCCs. The pairwise comparison of $\Delta\mu_s'(\lambda)$ between actinic keratosis with seborrheic keratosis, actinic keratosis with SCC, seborrheic keratosis with BCC, and seborrheic keratosis with SCC in the wavelength range between 455 and 765 nm was statistically significant.

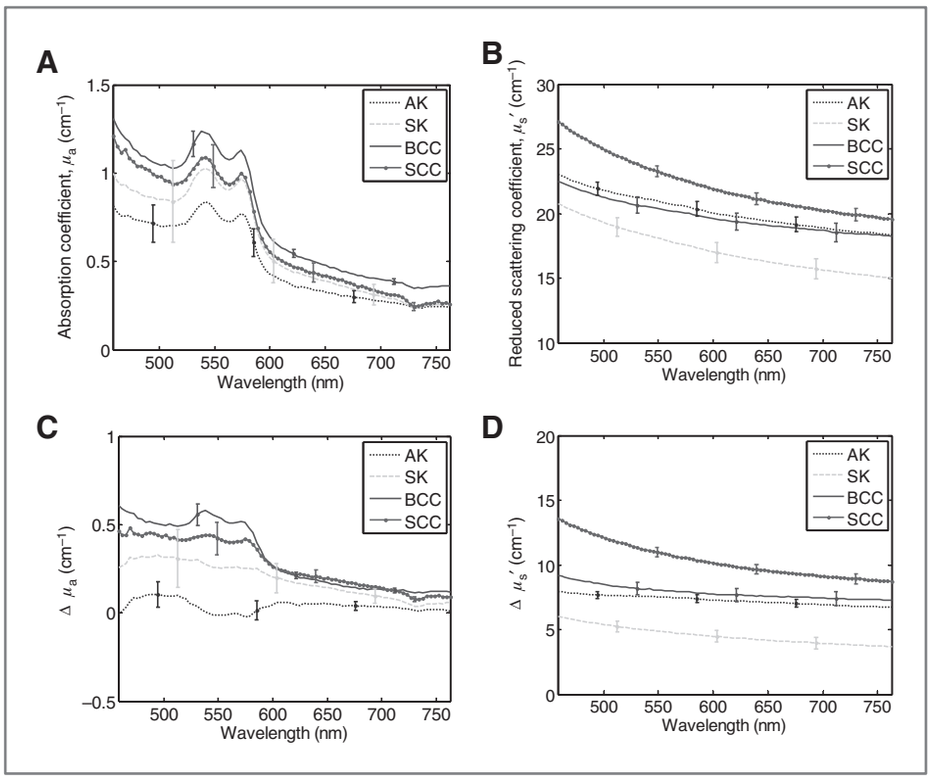

Figure 3. Average absorption coefficient spectra (A), average reduced scattering coefficient spectra (B), average differential absorption coefficient spectra (C), and average differential reduced scattering coefficient spectra (D) for SCCs, BCCs, actinic keratosis (AK), and seborrheic keratosis (SK). The error bars represent SEs.

This higher light scattering in cancerous cases can be explained by the larger average effective size of the scattering centers. SCC *in situ* has not yet penetrated through the basement membrane of the dermo-epidermal junction. SCCs typically appear as scaling plaques with sharply defined red color. Histologically, all epidermal layers may contain atypical keratinocytes. The larger amount of atypical keratinocytes in SCCs can increase the light scattering in this type of skin lesion and significantly affect its contribution to diffusely reflected light on the surface. SCCs may penetrate the basement membrane to become invasive. More advanced, invasive SCCs may appear clinically as hyperkeratosis and may ulcerate (40), which can affect the measurements of optical properties. To avoid this problem, we conducted the measurements in areas that did not present this condition.

Actinic keratosis may appear rough and scaly and may develop into a SCCs. Histologically, actinic keratoses are recognized by the presence of atypical keratinocytes in the deeper portions of the epidermis. Defective maturation of the superficial epidermal layers results in parakeratosis, alternating with hyperkeratosis (40, 41). During the data collection, we avoided areas that presented hyperkeratosis. The amounts of atypical keratinocytes and collagen are factors related to the amount of light scattering in the lesion.

BCCs are derived from the basal layer of keratinocytes, the deepest cell layer of the epidermis. BCCs can present nodular aggregates of basalioma cells in the dermis and exhibit peripheral palisading and retraction artifacts. Melanin can also be present in the tumor and in the surrounding stroma, as observed in pigmented BCCs. The aggregation of basalioma cells can increase the light scattering in these types of malignant lesions. The progression of seborrheic keratosis into BCC and SCC is rare (42, 43). However, seborrheic keratoses can clinically resemble SCCs, and for this reason, seborrheic keratoses are commonly removed or biopsied for histopathologic examination (44). Seborrheic keratoses, composed of basaloid cells admixed with some squamoid cells, can be pigmented when some cells contain melanin transferred from neighboring melanocytes.

The classifications of the skin lesions were carried out directly for the measured diffuse reflectance spectra. The advantage of using these direct measurements is that no homogeneity assumption is required. To design the classifiers, first we selected features from the diffuse reflectance spectra that effectively separated the malignant group from the benign group. The nature of the acquired diffuse reflectance spectra and what they represent played a role in determining their effectiveness. The characteristics of the diffuse reflectance data indicate that particular spectral regions have higher separability among the different classes. We used the continuous wavelet transform to extract the most effective features in the 2 classes under analysis (10). On the basis of the features, we investigated the use of multiple classification schemes to separate the skin lesions into clinically significant categories (benign, precancerous, and cancerous) as identified by their clinical and histopathologic diagnoses. The most successful classification scheme was ANN in combination with a genetic algorithm. For the pigmented and nonpigmented lesion groups, we classified the lesions into 2 classes at a time and repeated this for the subgroups, until we achieved the desired

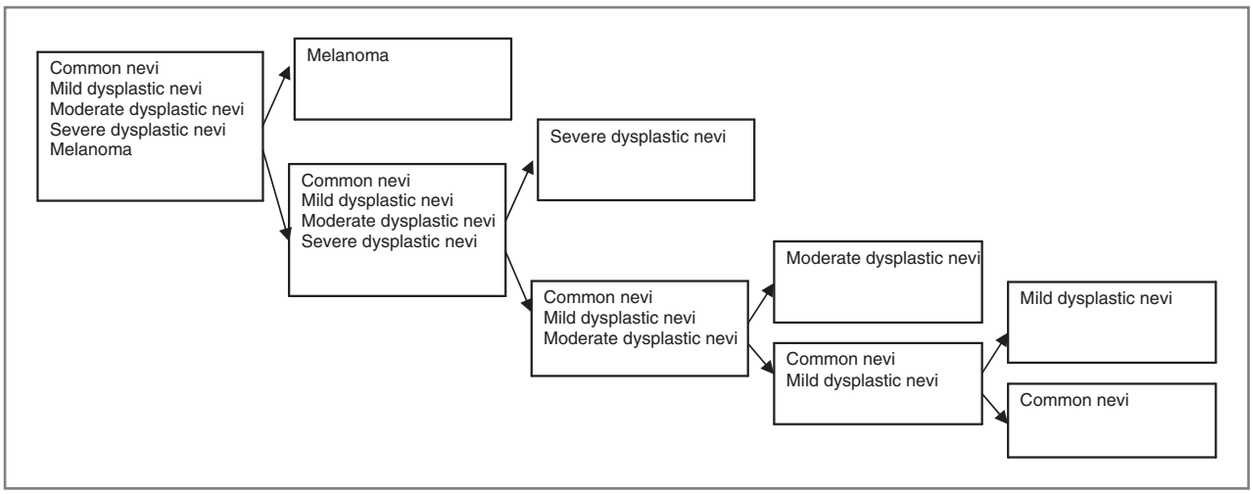

Figure 4. The classification scheme for pigmented lesions.

degree of categorization. Figure 4 illustrates the hierarchical classification system for pigmented lesions. This particular classification scheme intrinsically emphasizes the primary importance of accurate classification of melanoma and severe dysplastic nevi. Each stage consists of a single classifier. In the first stage, melanoma is separated from the other lesions. In a similar way, in each stage, the most "malignant" type lesion is separated from the remaining categories.

Table 1 presents the confusion matrixes for the training and testing sets, where the row headers show the ground truths from the histopathologic diagnosis and the column headers indicate the OIDRS classifications. The classification process in the testing set achieved 90% sensitivity and specificity for melanoma detection. Table 2 shows the sensitivity and specificity for each classifier in the hierarchical classification scheme. The minimum sensitivity is 89%, which corresponds to the classifiers that separate mild dysplastic nevi form benign common nevi. Sensitivity indicates the percentage of correctly identified positives (true positives) and specificity measures the proportion of negatives, which are correctly identified.

For the nonpigmented group, a single ANN classifier separated BCC and SCC from actinic keratosis and seborrheic keratosis. The designed classifier generated a sensitivity of 97% and a specificity of 96%. Table 3 shows the classification results for nonpigmented lesions. For the testing set, the sensitivity and specificity were both 92%.

Table 3. Nonpigmented lesions confusion matrix

	Predicted		
Actual	**BCC/SCC**	**AK/SK**	**Total**
Training			
BCC ($n = 78$)/SCC ($n = 49$)	123	4	127
AK ($n = 38$)/SK ($n = 12$)	2	48	50
Testing			
BCC ($n = 39$)/SCC ($n = 25$)	59	5	64
AK ($n = 19$)/SK ($n = 6$)	2	23	25

Abbreviations: AK, actinic keratosis; SK, seborrheic keratosis.

Conclusions

This study established that it is feasible to use OIDRS as a potential tool for *in vivo* discrimination of malignant cutaneous melanoma from other types of pigmented skin lesions. In a clinical trial, OIDRS distinguished malignant melanoma with 90% sensitivity and specificity for the testing set. The sensitivity and specificity for the training set were 100% and 95%, respectively. This system has also successfully classified BCCs and SCCs with 92% sensitivity and specificity. The sensitivity and specificity for the training set were 97% and 96%, respectively. Light scattering events inside the skin tissues change significantly with the development stage of the skin lesion. This change in the tissue scattering properties in the diffuse reflectance spectrum forms a physiologic basis for automated classification of different skin lesions based on OIDRS measurements.

Disclosure of Potential Conflicts of Interest

L.V. Wang has ownership interest (including patents). No potential conflicts of interest were disclosed by the other authors.

Authors' Contributions

Conception and design: A. Garcia-Uribe, J. Zou, M. Duvic, V.G. Prieto, L.V. Wang

Development of methodology: J. Zou, L.V. Wang

Acquisition of data (provided animals, acquired and managed patients, provided facilities, etc.): A. Garcia-Uribe, J. Zou, M. Duvic, V.G. Prieto

Analysis and interpretation of data (e.g., statistical analysis, biostatistics, computational analysis): A. Garcia-Uribe, J. Zou, M. Duvic, J.H. Cho-Vega, L.V. Wang

Writing, review, and/or revision of the manuscript: A. Garcia-Uribe, J. Zou, M. Duvic, J.H. Cho-Vega, V.G. Prieto, L.V. Wang

Administrative, technical, or material support (i.e., reporting or organizing data, constructing databases): A. Garcia-Uribe, J. Zou
Study supervision: J. Zou, M. Duvic, L.V. Wang
Identified the patients, made the clinical assessments, helped to design the study, and reviewed the images: M. Duvic

Acknowledgments

The authors thank Drs. Mays, Hymens, Mansfield, and the staff from the Melanoma and Skin Center at the University of Texas MD Anderson Cancer Center for their help during the data collection.

Grant Support

This project was sponsored by NIH grant R01 CA106728.

The costs of publication of this article were defrayed in part by the payment of page charges. This article must therefore be hereby marked *advertisement* in accordance with 18 U.S.C. Section 1734 solely to indicate this fact.

Received December 14, 2011; revised March 8, 2012; accepted March 26, 2012; published OnlineFirst April 5, 2012.

References

1. American Cancer Society. Melanoma skin cancer. http://www.cancer.org [cited 2011 Sep 10].
2. Williams ML, Sagebiel RW. Melanoma risk factors and atypical moles. West J Med 1994;160:343–50.
3. Cherpelis BS, Marcusen C, Lang PG. Prognostic factors for metastasis in squamous cell carcinoma of the skin. Dermatol Surg 2002;28:268–73.
4. Takata M, Saida T. Early cancers of the skin: clinical, histopathological, and molecular characteristics. Int J Clin Oncol 2005;10:391–7.
5. Zink D, Fischer AH, Nickerson JA. Nuclear structure in cancer cells. Nat Rev Cancer 2004;4:677–87.
6. Lelievre SA, Weaver VM, Nickerson JA, Larabell CA, Bhaumik A, Petersen OW, et al. Tissue phenotype depends on reciprocal interactions between the extracellular matrix and the structural organization of the nucleus. Proc Natl Acad Sci U S A 1998;95:14711–6.
7. Jorgensen P, Edgington NP, Schneider BL, Rupes I, Tyers M, Futcher B. The size of the nucleus increases as yeast cells grow. Mol Biol Cell 2007;18:3523–32.
8. Garcia-Uribe A, Smith EB, Zou J, Duvic M, Prieto V, Wang LV. *In-vivo* characterization of optical properties of pigmented skin lesions including melanoma using oblique incidence diffuse reflectance spectroscopy. J Biomed Opt 2011;16:020501.
9. Wallace VP, Bamber JC, Crawford DC, Ott RJ, Mortimer PS. Classification of reflectance spectra from pigmented skin lesions, a comparison of multivariate discriminant analysis and artificial neural networks. Phys Med Biol 2000;45:2859–71.
10. Garcia-Uribe A, Kehtarnavaz N, Marquez G, Prieto V, Duvic M, Wang LV. Skin cancer detection by spectroscopic oblique-incidence reflectometry: classification and physiological origins. Appl Opt 2004;43:2643–50.
11. McIntosh LM, Summers R, Jackson M, Mantsch HH, Mansfield JR, Howlett M, et al. Towards non-invasive screening of skin lesions by near-infrared spectroscopy. J Invest Dermatol 2001;116:175–81.
12. Sigurdsson S, Philipsen PA, Hansen LK, Larsen J, Gniadecka M, Wulf HC. Detection of skin cancer by classification of Raman spectra. IEEE Trans Biomed Eng 2004;51:1784–93.
13. Gniadecka M, Philipsen PA, Sigurdsson S, Wessel S, Nielsen OF, Christensen DH, et al. Melanoma diagnosis by Raman spectroscopy and neural networks: structure alterations in proteins and lipids in intact cancer tissue. J Invest Dermatol 2004;122:443–9.
14. Lynn CJ, Saidi IS, Oelberg DG, Jacques SL. Gestational age correlates with skin reflectance in newborn infants of 24–42 weeks gestation. Biol Neonate 1993;64:69–75.
15. Moncrieff M, Cotton S, Claridge E, Hall P. Spectrophotometric intracutaneous analysis: a new technique for imaging pigmented skin lesions. Br J Dermatol 2002;146:448–57.
16. Tomatis S, Carrra M, Bono A, Bartoli C, Lualdi M, Tragni G, et al. Automated melanoma detection with a novel multispectral imaging system: results of a prospective study. Phys Med Biol 2005;50:1675–87.
17. Arifler D, Schwarz RA, Chang SK, Richards-Kortum R. Reflectance spectroscopy for diagnosis of epithelial precancer: model-based analysis of fiber-optic probe designs to resolve spectral information from epithelium and stroma. Appl Opt 2005;44:4291–305.
18. Bargo PR, Pral SA, Goodell TT, Sleven RA, Koval G, Blair G, et al. *In-vivo* determination of optical properties of normal and tumor tissue with white light reflectance and an empirical light transport model during endoscopy. J Biomed Opt 2005;10:034018.
19. Mayinger B, Horner P, Jordan M, Gerlach C, Horbach T, Hohenberger W, et al. Endoscopic fluorescence spectroscopy in the upper GI tract for the detection of GI cancer: initial experience. Am J Gastroenterol 2001;96:2616–21.
20. Georgakoudi I, Jacobson BC, Van Dam J, Backman V, Wallace MB, Muller MG, et al. Fluorescence, reflectance, and light-scattering spectroscopy for evaluating dysplasia in patients with Barrett's esophagus. Gastroenterology 2001;120:1620–9.
21. Dacosta RS, Wilson BC, Marcon NE. Light-induced fluorescence endoscopy of the gastrointestinal tract. Gastrointest Endosc Clin N Am 2000;10:37–69.
22. Dacosta RS, Wilson BC, Marcon NE. New optical technologies for earlier endoscopic diagnosis premalignant gastrointestinal lesions. J Gastroenterol Hepatol 2002;17 Suppl:S85–104.
23. Mirabal YN, Chang SK, Atkinson EN, Malpica A, Malpica A, Follen M, Richards-Kortum R. Reflectance spectroscopy for *in-vivo* detection of cervical precancer. J Biomed Opt 2002;7:587–94.
24. Ramanujam N, Mitchell MF, Mahadevan A, Warren S, Thomsen S, Silva E, et al. *In-vivo* diagnosis of cervical intraepithelial neoplasia using 337-nm-excited laser-induced fluorescence. Proc Natl Acad Sci U S A 1994;91:10193–7.
25. Nath A, Rivoire K, Chang S, West L, Cantor SB, Basen-Engquist K, et al. A pilot study for a screening trial of cervical fluorescence spectroscopy. Int J Gynecol Cancer 2004;14:1097–107.
26. Johnson KS, Chicken DW, Pickard DC, Lee AC, Briggs G, Falzon M, et al. Elastic scattering spectroscopy for intraoperative determination of sentinel lymph node status in the breast. J Biomed Opt 2004;9:1122–8.
27. Fantini S, Walker SA, Franceschini MA, Kaschke M, Schlag PM, Moesta KT. Assessment of the size, position, and optical properties of breast tumors in-vivo by noninvasive optical methods. Appl Opt 1998;37:1982–9.
28. Tadrous PJ, Siegel J, French PM, Shousha S, Lalani el-N, Stamp GW. Fluorescence lifetime imaging of unstained tissues: early results in human breast cancer. J Pathol 2003;199:309–17.
29. Zonios G, Dimou A. Light scattering spectroscopy of human skin *in-vivo*. Opt Express 2009;17:1256–67.
30. Gillenwater A, Jacob R, Richards-Kortum R. Fluorescence spectroscopy: a technique with potential to improve the early detection of aerodigestive tract neoplasia. Head Neck 1998;20:556–62.
31. Müller MG, Valdez TA, Georgakoudi I, Backman V, Fuentes C, Kabani S, et al. Spectroscopic detection and evaluation of morphologic and biochemical changes in early human oral carcinoma. Cancer 2003;7:1681–92.
32. Richards-Kortum R, Sevick-Muraca E. Quantitative optical spectroscopy for tissue diagnosis. Annu Rev Phys Chem 1996;47:555–606.
33. Haykin AS. Neural networks expand SP's horizons. IEEE Signal Process Magn 1996;13:24–49.
34. Shea CR, Vollmer RT, Prieto VG. Correlating architectural disorder and cytologic atypia in Clark (dysplastic) melanocytic nevi. Hum Pathol 1999;30:500–5.
35. Wang L-H, Jacques SL. "Analysis of diffusion theory and similarity relations", in photon migration and imaging in random media and tissues. Proc Soc Photo-Opt Instrum Eng 1993;1888:107–16.
36. Kienle A, Patterson MS. Determination of the optical properties of turbid media from a single Monte-Carlo simulation. Phys Med Biol 1996;41:2221–7.

37. Mourant JR, Freyer JP, Hielscher AH, Eick AA, Shen D, Johnson TM. Mechanisms of light scattering from biological cells relevant to noninvasive optical-tissue diagnostics. Appl Opt 1998;37:3586–93.

38. Mourant JR, Canpolat M, Brocker C, Esponda-Ramos O, Johnson TM, Matanock A, et al. Light scattering from cells: the contribution of the nucleus and the effects of proliferative status. J Biomed Opt 2000;5:131–7.

39. Elder David E. Precursors to melanoma and their mimics: nevi of special sites. Mod Pathol 2006;19:S4–20.

40. Anwar J, Wrone DA, Kimyai-Asadi A, Alam M. The development of actinic keratosis into invasive squamous cell carcinoma: evidence and evolving classification schemes. Clin Dermatol 2004;22:189–96.

41. Goldberg LH, Joseph AK, Tschen JA. Proliferative actinic keratosis. Int J Dermatol 1994;33:341–5.

42. Mikhail GR, Mehregan AH. Basal cell carcinoma in seborrheic keratosis. J Am Acad Dermatol 1982;6:500–6.

43. Sloan JB, Jaworsky C. Clinical misdiagnosis of squamous cell carcinoma *in-situ* as seborrheic keratosis. A prospective study. J Dermatol Surg Oncol 1993;19:413–6.

44. Duque MI, Jordan JR, Fleischer AB, Williford PM, Feldman SR, Teuschler H, et al. Frequency of seborrheic keratosis biopsies in the United States: a benchmark of skin lesion care quality and cost effectiveness. Dermatol Surg 2003;29:796–801.